

Article

Experimental Research and Theoretical Analysis of the Coupling Mechanism Between Microstructure and Acoustics in Porous Materials

Haoshuai Suo ^{1,2}, Junhuai Xu ^{2,3}, Yaohan Feng ², Dongsheng Liu ², Pei Tang ^{1,*} and Ya Feng ^{2,*}

¹ State Key Laboratory of Silicate Materials for Architectures, Wuhan University of Technology, Wuhan 430070, China; shs95212022@163.com

² China Southwest Architecture Design and Research Institute Co., Ltd., CSCEC Green Construction Engineering Research Center, Chengdu 610041, China; xujunhuaiup@163.com (J.X.); 18223193710@163.com (Y.F.); s9386@whut.edu.cn (D.L.)

³ CSWADI (Sichuan) Science and Technology Co., Ltd., Chengdu 610041, China

* Correspondence: pei-tang@whut.edu.cn (P.T.); xnyjd2@vip.163.com (Y.F.)

Abstract: Based on the three-parameter approximate JCAL analytical model (hereinafter referred to as the three-parameter model), this study conducted an in-depth analysis of the effects of porosity, median pore size, and pore size standard deviation on the acoustic performance of porous materials and developed a composite porous material composed of glass fibers and zeolite particles. Experimental results indicate that the pore size distribution significantly affects the acoustic performance of fibrous porous sound-absorbing materials. Specifically, smaller pores lead to better sound absorption at mid–low frequencies, with the optimal sound absorption performance observed when the median pore size is between 60 and 80 μm . Increasing the material density and decreasing the fiber diameter help reduce the internal pore size, thereby improving the material’s sound absorption performance. Additionally, the appropriate addition of zeolite can further optimize the internal pore size and effective sound-absorbing interface, thus enhancing the material’s sound absorption performance. When the material density is 120 kg/m^3 and the zeolite substitution rate is around 10%, the material exhibits the best acoustic performance, with a noise reduction coefficient (NRC) reaching 0.65, which is a 10.17% increase compared to the material without zeolite. Comparing the simulation data from the three-parameter model with the actual measurement data shows that the model has excellent predictive performance for the sound absorption coefficient (SAC) of single-fiber porous materials (with an error of approximately 5%). However, for composite porous materials, due to the complex changes in interfaces, there is a certain prediction error (with the maximum error reaching 12.81%), indicating that the model needs further optimization and correction when applied to composite materials.

Keywords: composite materials; sound absorption; pore size distribution; fiber diameter; inorganic particles



Academic Editor: John S. Allen

Received: 10 February 2025

Revised: 2 March 2025

Accepted: 10 March 2025

Published: 13 March 2025

Citation: Suo, H.; Xu, J.; Feng, Y.; Liu, D.; Tang, P.; Feng, Y. Experimental Research and Theoretical Analysis of the Coupling Mechanism Between Microstructure and Acoustics in Porous Materials. *Appl. Sci.* **2025**, *15*, 3104. <https://doi.org/10.3390/app15063104>

Copyright: © 2025 by the authors. Licensee MDPI, Basel, Switzerland.

This article is an open access article distributed under the terms and conditions of the Creative Commons Attribution (CC BY) license (<https://creativecommons.org/licenses/by/4.0/>).

1. Introduction

With the continuous development of industrialization and urbanization, the surge in traffic volume, frequent construction activities, operation of industrial equipment, and the rise in recreational activities has significantly increased noise generation [1,2]. Noise pollution has become a focal issue across multiple fields and disciplines. Researchers from various domains, including materials science [3–5], environmental

engineering [6–9], architectural design [10,11], and urban planning [12–14], are actively exploring more effective noise absorption and reduction materials.

Among various sound-absorbing materials, fiber-based porous materials are widely used in noise reduction due to their elongated morphology, which provides a high specific surface area and an open, continuous pore structure. However, these materials typically exhibit less effective sound absorption at mid-to-low frequencies compared to high frequencies, which limits their application scope. To address this limitation, significant efforts have been devoted to the design and fabrication of porous sound-absorbing materials, including modifications to fiber surface roughness [15], gradient pore structures [16–18], folded structures [19], and fiber cross-sectional shapes [20]. In recent years, porous composite materials [21–23] have garnered widespread attention due to their excellent physical properties, non-flammability, and acoustic performance. Fiber–granular composites are a new category of porous composite materials that are composed of granular material embedded in a fibrous matrix. These materials are typically lightweight, highly porous, and cost-effective. By leveraging the complementary sound absorption properties of different components and optimizing their overall acoustic performance through diverse structural and material combinations, fiber–granular composites demonstrate superior acoustic properties compared to single-component fiber or particle-based porous materials. However, the underlying mechanisms of fiber–particle composites in acoustics are limited in research.

In order to delve into the propagation characteristics of sound waves in different media and to better predict the acoustic performance of materials, numerous scholars have established sound absorption models. To date, research on fiber-based porous materials has primarily focused on D-B type empirical models [24–27] and Johnson–Champoux–Allard (JCA) type semi-phenomenological models [28–32], analyzing parameters such as porosity, flow resistivity, viscous characteristic length, thermal characteristic length, and tortuosity. Generally, models with a larger number of parameters are better equipped to accurately describe the dissipation of acoustic energy within porous media, thus enabling more precise predictions of their sound absorption coefficients. However, the inclusion of more parameters increases the complexity of the models. Some of these parameters are extremely challenging to measure directly and are often inferred from fitted data, which poses certain challenges for studying the microstructure of porous media.

In recent years, Horoshenkov et al. [33] demonstrated through theoretical and experimental studies that the acoustic impedance of porous media with a pore size distribution approximating a log-normal distribution can be predicted using only three parameters: porosity, median pore size, and the standard deviation of the pore size. This significantly simplifies the process of predicting the acoustic characteristics of porous media. Considering complexity and prediction accuracy, the three-parameter model is one of the most ideal models for sound absorption performance prediction, and it is widely used in the prediction of the sound absorption performance of foam [34,35] and particle [36,37] porous materials. However, the application of the three-parameter model in fiber and its composite porous sound absorption materials is limited. Hurrell [38] used this model to predict the acoustic behavior of nanofiber membranes, expanding the understanding of the relationship between the acoustic properties of nanofiber media and related non-acoustic characteristics; Begum [39] utilized the three-parameter model to elucidate the high sound absorption and thermal insulation performance of fiber felts impregnated with aerogel powders, thereby extending the application of the three-parameter model to the field of composite materials. Nevertheless, the empirical application and verification research using this model to link the acoustic characteristics of fibrous porous media with the pore size of fibrous porous

materials is still insufficient. The specific impact of characteristic pore size on the acoustic performance of fibrous porous materials requires further in-depth research.

To further verify the applicability of the three-parameter model to fibrous composite porous sound-absorbing materials and to supplement the empirical research on the relationship between the acoustic performance and characteristic dimensions of fibrous and particulate composite porous sound-absorbing materials, this study also aims to develop a composite material with good sound absorption performance in the mid-to-low frequency range. Based on the three-parameter model, this paper analyzes the effects of fiber diameter and pore size distribution on the sound absorption performance of porous materials and prepares and optimizes a new type of porous sound-absorbing material composed of glass fibers and inorganic particles. The goal is to enhance the material's sound absorption performance in the mid-to-low frequency range without increasing the material thickness, thereby overcoming the deficiency of the weak low-frequency sound absorption performance of single-glass-fiber materials.

2. Model Analysis

The predictive model used in this study is the Horoshenkov three-parameter model [33], which simplifies the JCAL six-parameter model by expressing the two characteristic lengths and two permeability parameters in terms of the median pore size and the standard deviation of the pore size. Specifically, the model is expressed as follows [33]:

$$\Lambda = \bar{s}e^{-\frac{5}{2}(\sigma_s \log 2)^2} \quad (1)$$

$$\Lambda' = \bar{s}e^{\frac{3}{2}(\sigma_s \log 2)^2} \quad (2)$$

$$k_0 = \frac{\bar{s}^2 \varphi}{8\alpha_\infty} e^{-6(\sigma_s \log 2)^2} \quad (3)$$

$$k'_0 = \frac{\bar{s}^2 \varphi}{8\alpha_\infty} e^{6(\sigma_s \log 2)^2} \quad (4)$$

$$\alpha_\infty = e^{4(\sigma_s \log 2)^2} \quad (5)$$

where φ is the porosity, \bar{s} is the median pore size, σ_s is the standard deviation of pore size, Λ is the viscous characteristic length, Λ' is the thermal characteristic length, k_0 is the viscous flow resistance, k'_0 is the thermal flow resistance, and α_∞ is the tortuosity factor.

Compared to other semi-phenomenological models, this model requires fewer parameters (the complete formula of the three-parameter model is shown in Supplementary Materials S1), and key parameters such as porosity, median pore size, and pore size standard deviation can be directly measured. This significantly simplifies the process of predicting acoustic performance. Furthermore, its predictions are almost identical to those of the Johnson–Champoux–Allard–Lafarge (JCAL) model.

To thoroughly investigate the specific effects of three key parameters—porosity, average pore diameter, and pore diameter standard deviation—on the sound absorption performance of materials, this section employs COMSOL Multiphysics 6.1 software for simulation analysis. A three-dimensional (3D) finite element model of porous materials was developed using the Pressure Acoustics module, as illustrated in Figure 1. The model incorporates both the air layer and porous material section of an impedance tube, complete with mesh generation and sensor field point establishment. The impedance tube configuration features a plane wave radiation source at one end and a rigid wall boundary condition at the opposite end. The porous medium acoustic model utilizes the three-parameter approximation “JCAL” model. The simulation encompasses 626 frequency points from 50 to 6300 Hz with 10 Hz increments, during which parametric sweeps were conducted for

material porosity, average pore diameter, and pore diameter standard deviation to comprehensively analyze their individual and combined effects on sound absorption performance.

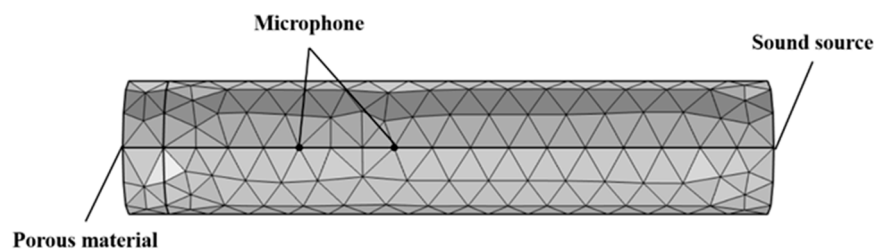


Figure 1. Finite element model diagram.

To simulate the acoustic performance of actual fiber porous materials, specific parameter ranges were defined based on a previous actual test. The porosity was set within the range of 90–98%, the median pore size ranged from 40 μm to 120 μm , and the pore size standard deviation ranged from 0.1 to 0.3, as shown in Table 1. The thickness of the studied materials was fixed at 3 cm, and the sound absorption performance was calculated over the frequency range of 50–6300 Hz. When analyzing the effect of a single parameter on sound absorption performance, the other two parameters were set to the midpoint of their respective ranges to eliminate interference.

Table 1. Ranges of different parameters.

porosity	0.90	0.92	0.94	0.96	0.98
median pore size (μm)	40	60	80	100	120
standard deviation in pore size distribution	0.10	0.15	0.20	0.25	0.30

The sound absorption performance after parameterized scanning of different factors is shown in Figure 2. Figure 2a–c illustrates the effects of changes in porosity, pore size standard deviation, and median pore size on the sound absorption coefficient, respectively, while Figure 2d–f depicts the corresponding noise reduction coefficient (NRC) and average sound absorption coefficient (AAC). Within the specified parameter ranges, when the material’s porosity exceeds 90%, the sound absorption performance remains relatively stable across different porosities, indicating that changes in porosity have a limited impact on sound absorption performance under these conditions. For glass-fiber-based porous materials, prior experiments have shown that under uniform material conditions, the pore size standard deviation remains below 0.3 and varies between 0.1 and 0.3. As observed in the figures, within this range, the NRC shows a gradual increase as the pore size standard deviation increases. Simultaneously, the peak sound absorption coefficient slightly decreases, while the mid-to-low frequency sound absorption coefficients slightly improve. Overall, the average sound absorption coefficient exhibits no significant change. However, a moderate broadening of the pore size distribution is beneficial for enhancing the mid-to-low frequency sound absorption performance of porous materials.

Compared to porosity and pore size standard deviation, changes in median pore size have a more significant impact on sound absorption performance. The two-dimensional curves of sound absorption coefficients under changes in median pore size can be found in Figure S1. As the median pore size increases, the frequency of the first peak in the sound absorption coefficient shifts slightly toward higher frequencies, and the peak sound absorption coefficient first increases and then decreases. This indicates that under the same porosity and pore size standard deviation, smaller median pore sizes are beneficial for low-frequency sound absorption performance [3]. However, excessively small pore

sizes can lead to a reduction in overall sound absorption performance. This phenomenon occurs because smaller pore sizes result in a higher number of fibers per unit area, increasing the likelihood of sound waves colliding with the fiber surfaces within the material. Consequently, the friction between sound waves and the air within the material increases, prolonging the propagation time of the sound waves inside the material and converting a substantial amount of acoustic energy into thermal energy, leading to its dissipation. However, overly small pore sizes can significantly increase the material's density, leading to excessively high flow resistivity. This, in turn, causes a large amount of sound wave reflection, negatively affecting the acoustic performance of the material [40].

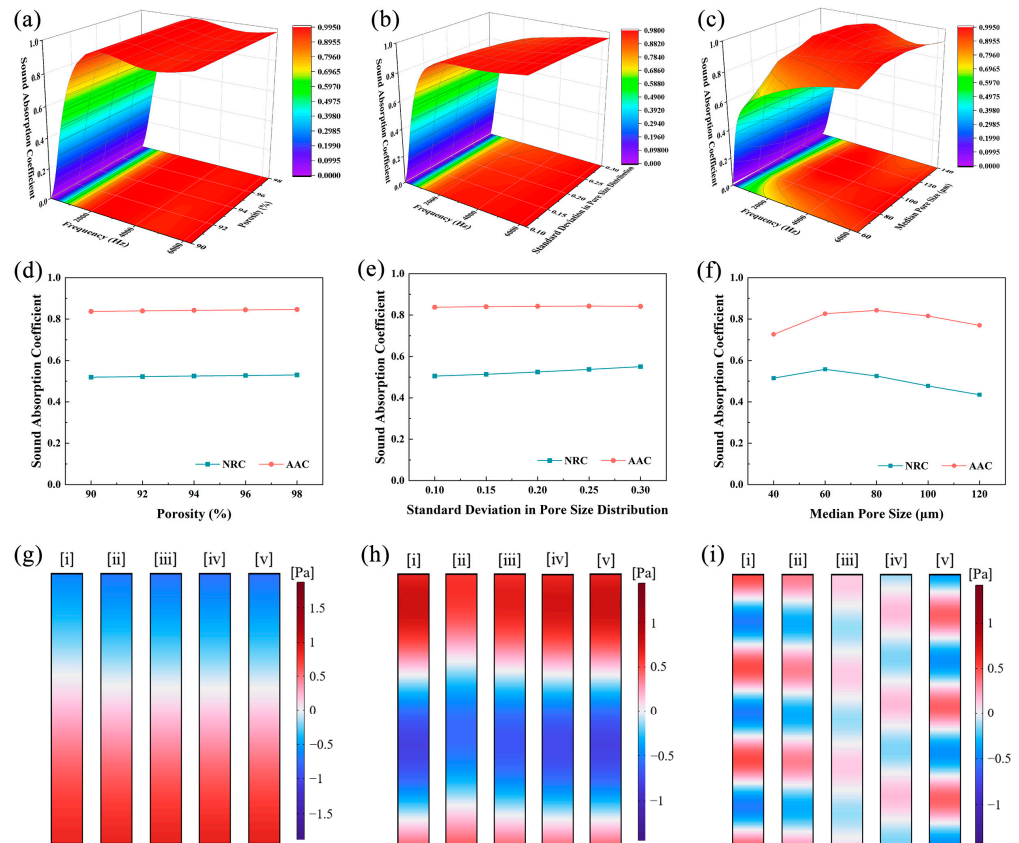


Figure 2. Effects of different parameters on the sound absorption coefficient: (a) porosity, (b) standard deviation of pore size, (c) median pore size; effects of parameter variations on NRC and average sound absorption coefficient: (d) porosity, (e) standard deviation of pore size, (f) median pore size; pressure acoustics simulation results: (g) 280 Hz, (h) 800 Hz, (i) 2500 Hz, where (i–v) represent the scattered pressure fields for median pore sizes of 40 μm , 60 μm , 80 μm , 100 μm , and 120 μm , respectively.

To intuitively demonstrate the impact of median pore size on sound propagation behavior, simulation results for representative frequencies in the low-, medium-, and high-frequency ranges—280 Hz, 800 Hz, and 2500 Hz—were compared. Figure 2g–i shows the scattered sound pressure fields in the absorption domain under different median pore sizes. In the scattered sound pressure maps, red and dark blue regions represent areas of high sound pressure [41], with color intensity reflecting the strength of sound wave energy. By comparing the scattered sound pressure fields at the same frequency but with different pore sizes, it can be observed that the degree of attenuation in scattered sound pressure varies. At low frequencies, smaller pore sizes result in weaker scattered sound pressures, indicating that at these frequencies, smaller pores lead to more complete absorption of the incident sound waves. As the frequency increases, excessively small pore sizes exhibit

higher scattered sound pressures compared to other pore sizes. When the median pore size is 80 μm , the scattered sound pressure at 2500 Hz is nearly zero, indicating that the incident sound wave is almost completely absorbed. This suggests that there is an optimal range for median pore size. Combined with Figure 2f, which depicts the NRC and the average sound absorption coefficient, it can be concluded that a median pore size in the range of 60–80 μm achieves the best sound absorption performance.

3. Materials and Methods

3.1. Materials and Preparation

In this study, glass fibers with diameters of 5 μm and 7 μm were selected, along with potassium silicate (AR) and zeolite particles (74 μm). The densities of the glass fibers and zeolite particles were 2491.7 kg/m^3 and 1100 kg/m^3 , respectively. The main chemical compositions of the materials are shown in Table 2.

Table 2. Chemical composition of glass fiber and zeolite raw materials (wt%).

	Na ₂ O	MgO	Al ₂ O ₃	SiO ₂	SO ₃	K ₂ O	CaO	TiO ₂	Fe ₂ O ₃	P ₂ O ₅	MnO
Fiber	16.07	3.22	1.87	67.15	0.30	0.53	10.43	0.08	0.24	/	/
Zeolite	1.04	2.31	16.37	65.14	/	4.28	5.22	0.59	4.62	0.14	0.13

The glass fiber porous materials and composite materials were prepared using a lamination method. During the preparation process, a 20% concentration of potassium silicate solution was sprayed onto the surface of the glass fibers. The samples were then dried in an oven at 85 °C for 10 h to ensure complete drying and shaping. The composite fiber sound-absorbing materials were fabricated using the same molding method, with a layer of zeolite particles uniformly added between every two fiber layers. In this study, the thickness of the fiber porous materials was uniformly controlled at 30 mm. Five types of fiber porous materials with different densities (60 kg/m^3 , 80 kg/m^3 , 100 kg/m^3 , 120 kg/m^3 , and 140 kg/m^3) were prepared.

3.2. Experiment Test Method

3.2.1. Porosity Test Method

First, the volume and mass of the porous material are measured. The porosity of the porous sound-absorbing material, defined as the volume percentage occupied by the internal network structure, can be obtained by dividing the mass of the porous material by the mass of the dense solid corresponding to the porous material with the same volume as the material. The corresponding volume percentage of air is the porosity. To ensure accuracy, measurements should be taken at least three different positions for each sample, and the average values should be used. The calculation formula is as follows:

$$\varphi = \left(1 - \frac{M}{V\rho_s}\right) \times 100\% \quad (6)$$

where φ is porosity (%), M is the mass of the sample (kg), V is the volume of the sample (m^3), and ρ_s is the density of the corresponding dense solid material (kg/m^3).

For composite materials, the average density calculation method is applied to determine the porosity:

$$\varphi = \left(1 - \frac{M}{V\rho_0}\right) \times 100\% \quad (7)$$

Here, ρ_0 is the average density of the composite material, which can be calculated by the following formula:

$$\frac{1}{\rho_0} = \frac{\omega_{fiber}}{\rho_{fiber}} + \frac{\omega_{zeolite}}{\rho_{zeolite}} \quad (8)$$

where ω_{fiber} and $\omega_{zeolite}$ are the mass fraction of the glass fibers and zeolite particles, respectively, ρ_{fiber} is the density of the glass fibers, and $\rho_{zeolite}$ is the density of the zeolite particles.

3.2.2. Microscopic Morphology

In this experiment, the microscopic morphology and structure of the fiber porous materials and composite material samples were observed using a scanning electron microscope (SEM) (Zeiss Sigma 300). Additionally, the elemental composition of the porous materials was analyzed using energy-dispersive spectroscopy (EDS).

3.2.3. Pore Size Testing

- (1) Multiple SEM images of the same porous material were selected for pore size measurement. The pore sizes were determined by measuring the diameters of inscribed circles formed by fiber overlaps in the images, using ImageJ 1.54f software. The pore sizes were then statistically analyzed to calculate their distribution, and a pore size distribution chart was generated. The median pore size was calculated based on the measurements.
- (2) The median pore size and pore size distribution of the fiber porous materials were tested using a CFP-1500AE capillary pore size analyzer (Porous Materials Inc., Ithaca, NY, USA), following the ASTM F316-03 (2019) standard [42].

3.2.4. Measurement of Sound Absorption Coefficient

The sound absorption coefficient of the porous materials was measured using the two-microphone transfer function method. The setup consisted of an impedance tube (AWA8551 model), a multi-channel noise analysis tester (AWA6290M model), and pulse analysis software. The measurements were performed at a constant temperature ($23\text{ }^{\circ}\text{C} \pm 1\text{ }^{\circ}\text{C}$). The impedance tube system included two tubes:

A large tube with a diameter of 100 mm, used for testing absorption coefficients in the frequency range of 50–1600 Hz.

A small tube with a diameter of 20 mm, used for testing absorption coefficients in the frequency range of 500–6300 Hz.

The testing method complies with the national standard GB/T 18696.2-2002 [43], “Acoustics-Determination of sound absorption coefficient and impedance in impedance tubes-Part 2: Transfer-function method”. Figure S2 illustrates the schematic diagram of the sound absorption device.

Before testing, the AWA6223 sound calibrator (Hangzhou Aihua Instruments Co., Ltd., Hangzhou, China) was used to calibrate the sensors. The 1/3 octave band method was applied to measure the sound absorption coefficients. Three samples were tested for each density, and each sample was measured three times. The average value of these measurements was taken as the sound absorption coefficient for that type of sample. The testing frequency range was 50–6300 Hz.

The noise reduction coefficient (NRC) was determined according to the American standard ASTM C634-13 (2021) [44]. NRC is calculated as the average of the 1/3 octave band sound absorption coefficients at 250 Hz, 500 Hz, 1000 Hz, and 2000 Hz, using the following formula:

$$\text{NRC} = \frac{\alpha_{250} + \alpha_{500} + \alpha_{1000} + \alpha_{2000}}{4} \quad (9)$$

4. Results and Discussion

4.1. Morphology and Porosity Structure of Porous Materials

4.1.1. Morphology and Pore Size Distribution of Single-Fiber Porous Materials

The morphology of the fiber porous material is shown in Figure 3a. Observations reveal that fine particles are attached to the fiber surfaces, giving them a rough texture (the detailed microscopic surface morphology images of the fibers are presented in Figure S3). The fibers are bonded to each other through potassium silicate (spot analyses by EDS revealed the presence of K in these particles; see Table S1 for details), forming interconnected pores. These pores act as transmission channels for sound waves to enter the material. When sound waves penetrate the porous material, they continuously collide with the fiber surfaces and undergo friction with the pore walls and air molecules. These interactions, combined with multiple reflections and refractions within the porous structure, lead to significant energy dissipation, thereby enhancing the material's sound absorption performance.

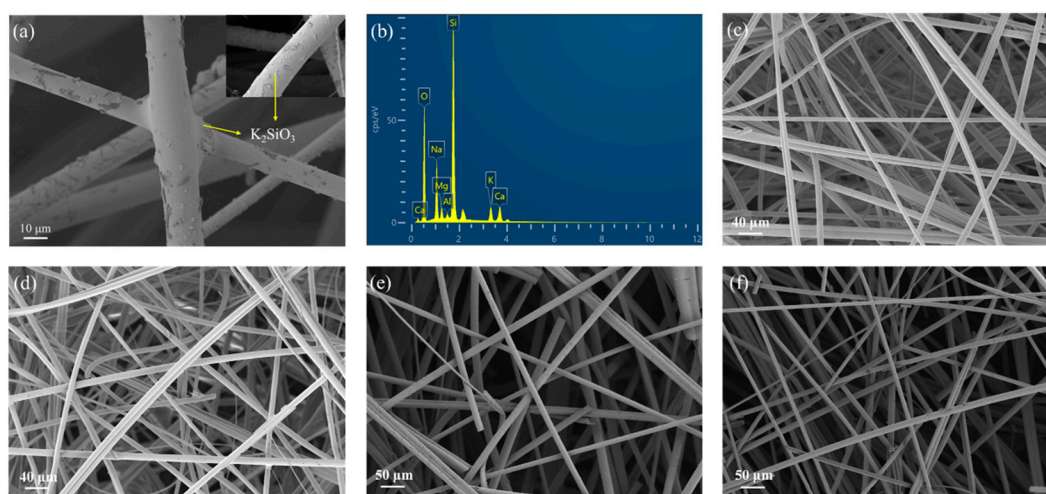


Figure 3. Microscopic morphology of fibrous porous materials: (a) Microscopic image of fiber interlocking, (b) EDS analysis, (c) 7 μm diameter, 80 kg/m^3 , (d) 7 μm diameter, 100 kg/m^3 , (e) 7 μm diameter, 80 kg/m^3 , (f) 5 μm diameter, 80 kg/m^3 .

For fibers with the same diameter, taking the fiber with a diameter of 7 μm as an example, the pore size of the porous material decreases as the density increases, as shown in Figure 3c,d. Similarly, for a constant density, taking 80 kg/m^3 as an example, a reduction in fiber diameter also leads to smaller pore sizes, as shown in Figure 3e,f. It can be observed that decreasing the fiber diameter increases the number of fibers per unit area, resulting in tighter fiber overlaps. This increases the porosity and specific surface area of the porous material. Consequently, due to greater viscous losses and thermal losses [45], the dissipation of sound waves within the material becomes more significant.

From the SEM image in Figure 3, it can be observed that the pore structures formed by fiber intersections are highly complex. To analyze the pore size distribution of the porous material, the diameters of inscribed circles within the polygonal pores created by fiber overlaps were used to represent pore sizes [46]. SEM images of fiber porous materials with a fiber diameter of 7 μm at densities of 80 kg/m^3 , 100 kg/m^3 , and 120 kg/m^3 were imported into ImageJ software for analysis. Figure 4a–c shows the partial SEM top view of porous materials with 7 μm fiber diameters under three densities, respectively. These images reveal a large number of pores with varying sizes.

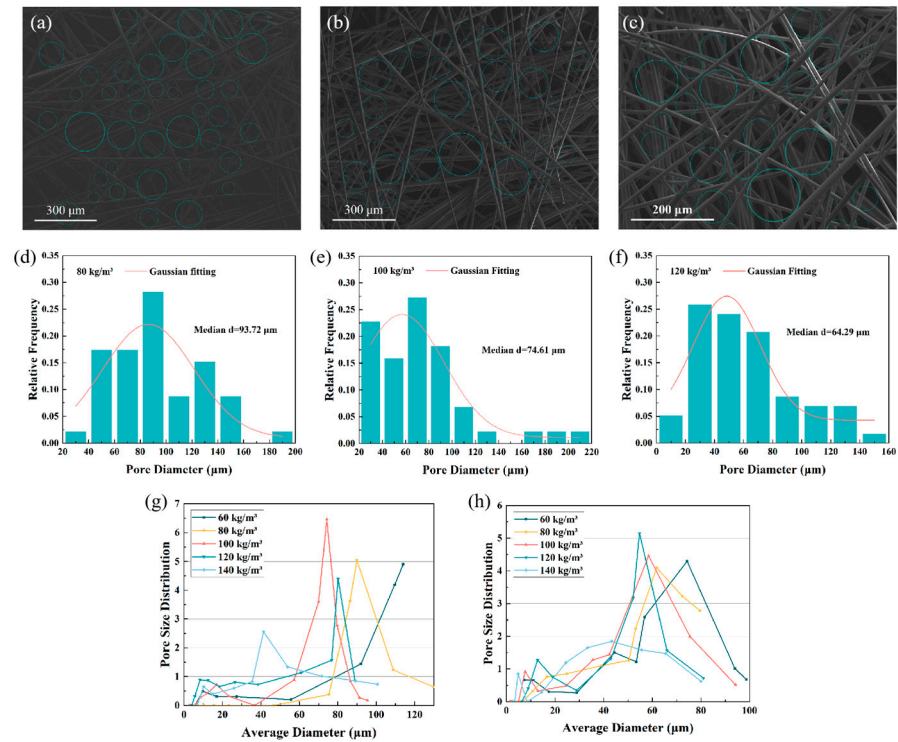


Figure 4. Pore size distribution of fibrous porous materials, where (a–c) are the SEM top views of the porous materials at density of 80 kg/m³, 100 kg/m³, and 120 kg/m³, respectively; (d–f) show the statistical results of their pore size distributions; and (g,h) illustrate the pore size distributions of porous materials with fiber diameters of 7 μm and 5 μm at different densities.

By measuring and statistically analyzing the diameters of the inscribed circles within the polygonal pores, the pore size distributions and median pore sizes of the fiber porous materials were obtained. The statistical results are shown in Figure 4d–f. It can be seen that as the density increases, the median pore size decreases progressively, which is consistent with the results of the SEM observation.

The pore size distribution of porous sound-absorbing materials was further tested by the capillary pore size analysis technique. The test results are shown in Figure 4g,h, where it can be observed that the pore size distribution of the fiber porous materials follows an approximately normal distribution, consistent with the application rules of the three-parameter analytical model [33]. Additionally, Table 3 lists the specific porosity and median pore size of the porous sound-absorbing materials. The pore size of the porous sound-absorbing materials primarily falls within the macropore range [47] (50 nm < pore size < 100 μm). As the density increases from 60 kg/m³ to 140 kg/m³, the median pore size of the materials gradually decreases, with a maximum reduction of 45.82%. A comparison of the median pore size obtained from the two testing methods (SEM and capillary pore size analysis) shows minimal deviation (maintain within 7%), confirming the accuracy of the measured median pore size in this study.

Table 3. Median pore size of single-fiber porous materials.

density		60	80	100	120	140
porosity (%)		97.59	96.79	95.98	95.18	94.38
median pore size (μm)	7 μm	97.6425	91.7545	76.7821	68.5024	52.9058
	5 μm	74.4599	69.4861	65.9613	58.1597	46.5611

4.1.2. Morphology and Pore Size Distribution of Composite Porous Materials

As previously mentioned, for materials with the same density, smaller fiber diameters result in better sound absorption performance. Therefore, in the optimization experiments, glass fibers with a diameter of 5 μm were chosen as the subject for optimization. By adding zeolite particles (200 mesh, 74 μm) to alter the pore structure of the fibrous porous material, composite porous materials were prepared to further optimize the sound absorption performance of the porous material.

Taking the density of 100 kg/m^3 as an example, the pore morphology of the composite porous materials is shown in Figure 5, which can be categorized into three distinct cases: zeolite particles uniformly dispersed within the fiber pores (10% addition), partial blockage of pores by zeolite particles (20% addition), and extensive blockage of fiber pores by zeolite particles (30% addition).

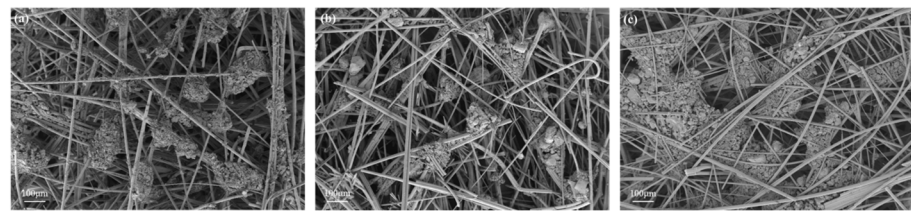


Figure 5. SEM images of different zeolite additions at 100 kg/m^3 : (a) 10%; (b) 20%; (c) 30%.

Figure 6 shows the median pore sizes and pore size distribution of porous materials with different zeolite addition levels across three densities (the median pore sizes for the remaining densities are provided in Table S2). It can be observed that at the same density, the median pore size of the porous material first increases and then decreases with the increase in zeolite replacement content. This phenomenon can be attributed to the fine particle characteristics of zeolite. At low replacement levels, zeolite particles partially substitute glass fibers, reducing the number of fibers required to form pores in the same volume. This results in a slight increase in the median pore size of the porous material. However, as the zeolite replacement level continues to increase, the excessive addition of zeolite particles leads to particle agglomeration and pore blockage within the material, as shown in Figure 5c. This causes the median pore size to decrease. These results clearly demonstrate that the addition of particles has a significant impact on the pore structure of fiber porous materials.

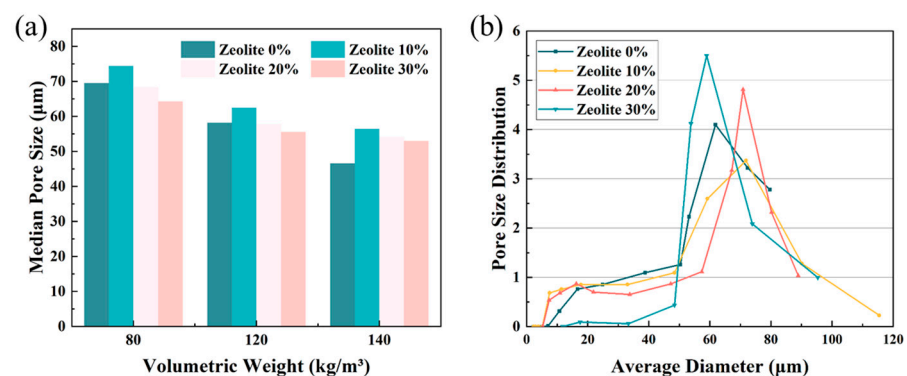


Figure 6. Cont.

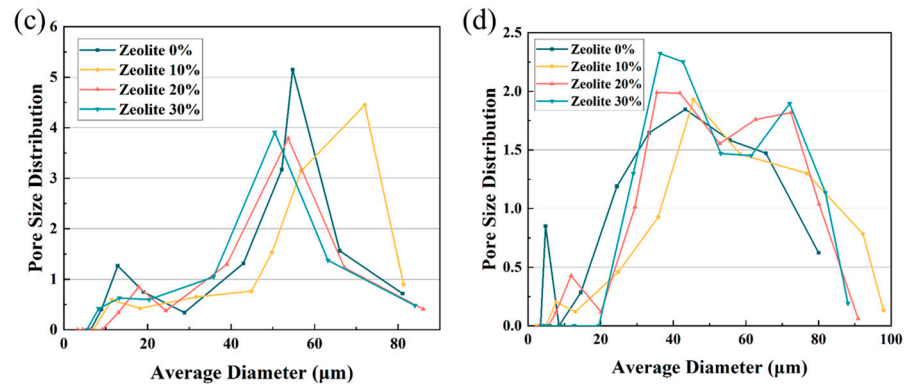


Figure 6. Pore size distribution of fibrous composite porous materials with different densities: (a) median pore size; (b) pore size distribution at 80 kg/m³; (c) pore size distribution at 100 kg/m³; (d) pore size distribution at 120 kg/m³.

4.2. Effect of Fiber Diameter on the Sound Absorption Performance of Porous Materials

Figure 7a,b illustrates the acoustic properties of porous materials made from fibers of two different diameters under varying densities as a function of frequency. Figure 8c summarizes the corresponding NRC results (the specific values of NRC can be found in Table S3). This study found that as density increases (leading to a reduction in pore size), the NRC first increases and then decreases. The sound absorption coefficient curves show that increasing the density improves the low- and mid-frequency sound absorption performance of fiber porous materials, while the high-frequency performance decreases. This trend is attributed to friction effects between the air and external pore walls (the surfaces of adjacent fibers) [14]. This phenomenon is more pronounced with fibers of smaller diameters. Due to the improvement in sound absorption performance at low frequencies and the decrease at high frequencies, the overall improvement in NRC between adjacent densities is not significant, with a maximum increase of 5.36%. The NRC reaches its maximum value at a density of 120 kg/m³, corresponding to median pore sizes of 68.50 µm and 58.16 µm for the two fiber diameters, respectively. When the density is 140 kg/m³, the median pore size further decreases, and the sound absorption performance declines. This suggests that the sound absorption performance of fiber-based porous materials in the low- and mid-frequency ranges improves as pore size decreases, but there exists an optimal pore size range. Exceeding this range can lead to reduced performance. This observation aligns well with the theoretical analysis presented in Section 2.

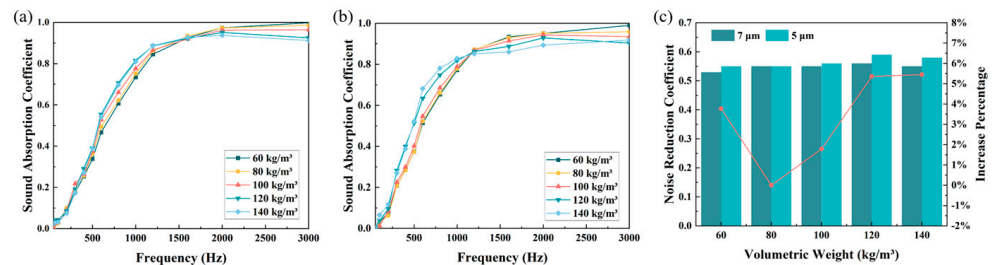


Figure 7. Sound absorption performance test results of single-fiber porous materials: (a) sound absorption coefficient of 7 µm fiber porous material; (b) sound absorption coefficient of 5 µm fiber porous material; (c) Percentage Increase.

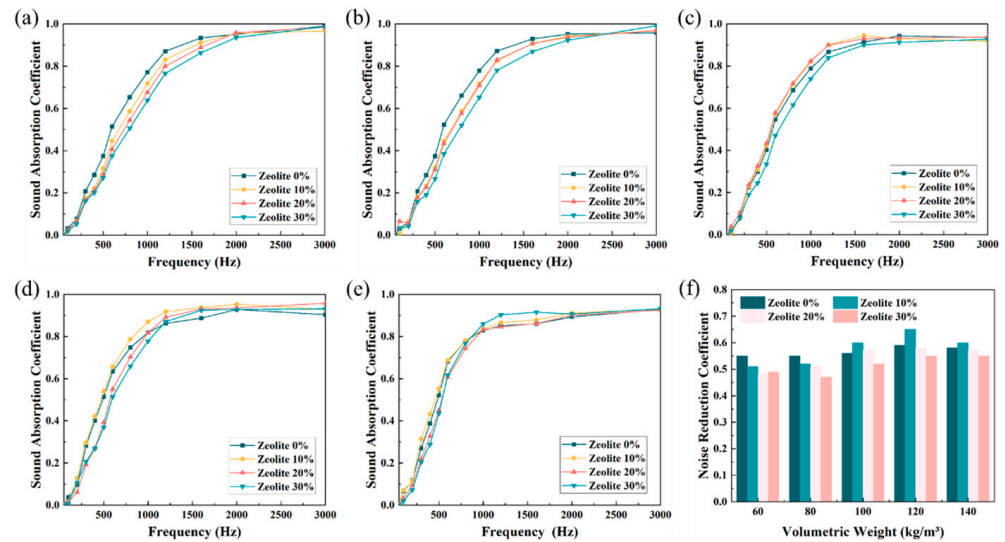


Figure 8. Sound absorption coefficient and NRC of composite materials under different densities: (a) 60 kg/m^3 ; (b) 80 kg/m^3 ; (c) 100 kg/m^3 ; (d) 120 kg/m^3 ; (e) 140 kg/m^3 ; (f) NRC.

Comparing the sound absorption coefficients of the two materials at the same density, it is evident that a reduction in fiber diameter results in smaller pore sizes and better sound absorption performance. This improvement is due to the increase in the contact area between the internal pores and air as the fiber diameter decreases, leading to more frequent collisions of sound waves with the material's surface, which enhances energy dissipation. Fiber porous materials with a diameter of $5 \mu\text{m}$ achieve a comparable sound absorption performance at a density of 60 kg/m^3 to that of fiber porous materials with a diameter of $7 \mu\text{m}$ at a density of 100 kg/m^3 . At this point, the median pore sizes of the two materials are also similar, further confirming that pore size significantly influences the sound absorption performance of fiber porous materials. As the pore size decreases, the sound absorption performance first improves and then diminishes, with an optimal pore size of approximately $60 \mu\text{m}$ exhibiting the highest sound absorption performance.

4.3. Effect of Lightweight Particles on the Sound Absorption Performance of Composite Porous Materials

Figure 8 shows the sound absorption coefficient curves for porous materials with varying amounts of zeolite added under five different densities, all prepared using fibers with a diameter of $5 \mu\text{m}$. Among them, Figure 8f summarizes the NRC for the various samples (the specific values are provided in Table S4). At lower densities (60 kg/m^3 and 80 kg/m^3), the addition of zeolite particles reduces the sound absorption performance of the porous materials, with the performance degradation becoming more pronounced as the zeolite content increases. Although the introduction of zeolite helps to form a favorable median pore size, the limited number of fibers at low densities combined with the substitution effect of zeolite prevents the formation of an effective space structure for sound absorption within the material. As a result, while sound waves may penetrate the material, they are less effectively dissipated, leading to reduced sound absorption performance. Furthermore, as the amount of zeolite increases, excessive zeolite particles tend to agglomerate (Figure 5c from Section 4.1), blocking the pores of the porous material and impairing its acoustic performance.

On the contrary, for higher densities ($\geq 100 \text{ kg/m}^3$), a small amount of zeolite substitution can enhance the sound absorption performance of the material. The improvement of sound absorption performance can be attributed to two main factors. On one hand, compared to low-density porous materials, higher-density materials contain a greater number

of fibers. This means that the substitution of fibers with a small amount of zeolite does not significantly reduce the structural complexity of the material. Instead, the addition of zeolite particles modifies the pore size distribution, creating an optimal pore size. The synergistic effect between the particles and fibers results in a significant pressure diffusion effect [48], thereby enhancing sound absorption performance. On the other hand, the addition of zeolite introduces two distinct interfaces within the porous material, due to the difference in acoustic impedance between these two interfaces, and sound waves undergo strong reflection and refraction as they transition from one interface to another. This process increases the dissipation of sound energy within the material, further improving its acoustic performance.

4.4. Model Validation

The sound absorption simulation of the 5 μm diameter fiber porous material was conducted at three densities: 80 kg/m^3 , 100 kg/m^3 , and 120 kg/m^3 . The results were then compared with the actual measurements, as shown in Figures 9–11. The experimental and simulated data for the single-fiber porous materials at these three densities showed a high degree of consistency, with errors maintained at about 5% (4.95%, 5.26%, and 5.88%, respectively). These results confirm the effectiveness of the three-parameter model in predicting the acoustic performance of single-fiber porous materials. However, for fiber-particle composite materials, the three-parameter model exhibits some deviation. At a density of 80 kg/m^3 , the composite material shows the maximum error of 12.81% when 30% zeolite particles are added. At densities of 100 kg/m^3 and 120 kg/m^3 , the maximum errors occur when the zeolite addition is 20%, with errors of 12.43% and 12.08%, respectively.

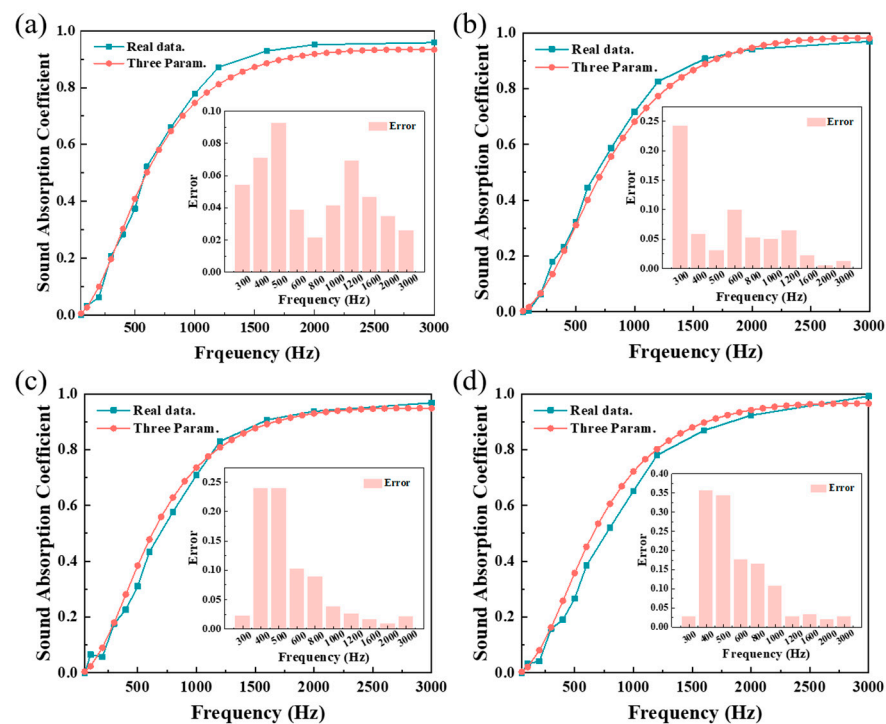


Figure 9. Comparison between the measured and simulated results of the sound absorption coefficient of porous materials with different zeolite additions at 80 kg/m^3 : (a) zeolite: 0%, (b) zeolite: 10%, (c) zeolite: 20%, (d) zeolite: 30%.

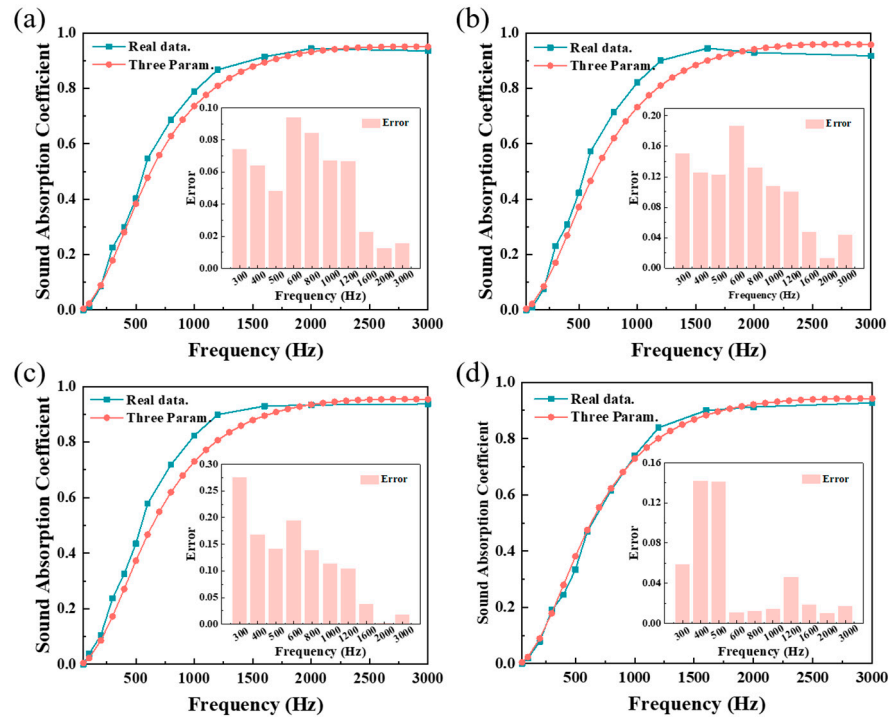


Figure 10. Comparison between the measured and simulated results of the sound absorption coefficient of porous materials with different zeolite additions at 100 kg/m^3 : (a) zeolite: 0%, (b) zeolite: 10%, (c) zeolite: 20%, (d) zeolite: 30%.

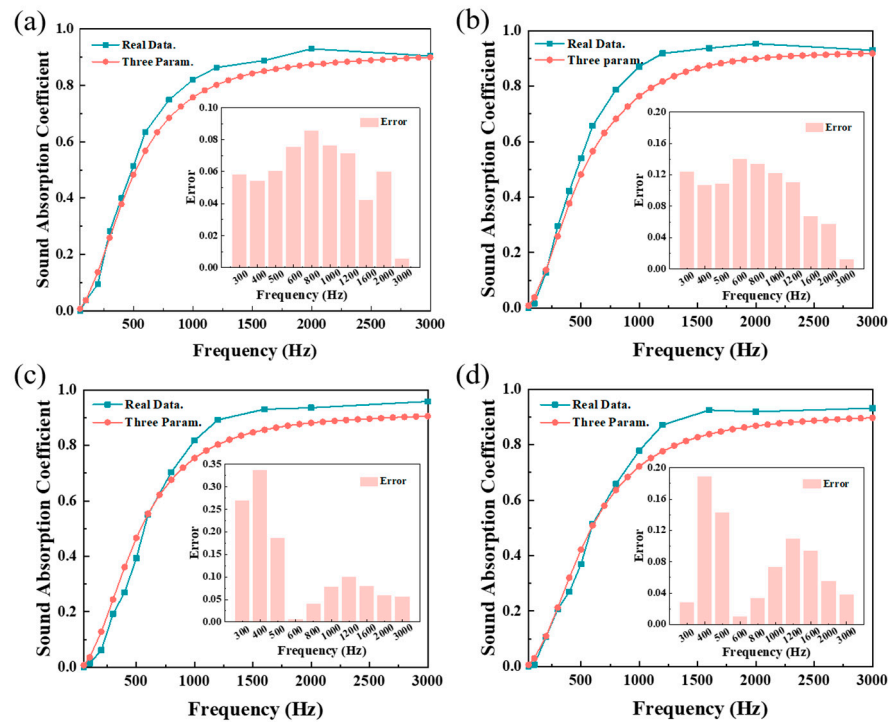


Figure 11. Comparison between the measured and simulated results of the sound absorption coefficient of porous materials with different zeolite additions at 120 kg/m^3 : (a) zeolite: 0%, (b) zeolite: 10%, (c) zeolite: 20%, (d) zeolite: 30%.

According to the statistical results, the error of the composite material in the mid-to-low frequency range is significantly greater than in the high-frequency range. For composite materials with a high amount of zeolite, the experimental values in the mid-to-low frequency range are generally lower than the simulated values, while for materials

with a small amount of zeolite, the experimental values are higher than the simulated ones. This is because high-frequency sound waves are primarily absorbed at the surface of the material, while low-frequency sound waves are absorbed deeper inside the material [49]. When a large amount of zeolite is added, the particles block the pores of the porous material, restricting the penetration and absorption of sound waves, leading to the low-frequency experimental sound absorption coefficients being lower than the simulated values. Conversely, when a small amount of zeolite is added, it does not obstruct sound wave penetration and creates a significant pressure diffusion effect, and the actual sound absorption effect will be higher than the simulation value. Thus, these are two distinct effects, resulting in larger errors in the low-frequency range compared to the high-frequency range. Additionally, the discrepancy may also be attributed to the unique layered structure of the composite porous material. As observed in the experiments, the composite material consists of multiple layers of ultrafine glass fibers and zeolite particles stacked together. During the stacking process, the uneven surfaces of the glass fiber layers and zeolite particle layers can introduce small air layers between the fiber layers, as illustrated in Figure 12a. Additionally, the presence of inorganic particles attached to the fiber layers further complicates the interface. Due to the reflection of sound waves at the boundary between the air layer and the sound-absorbing material layer, the sound wave is reduced by the interference of the wave in the air layer [50]. On a microscopic level, this layered structure can be conceptualized as numerous “three-layer” units composed of a “loose (fiber)–dense (fiber + zeolite particles)–loose (fiber)” structure. Additionally, Figure 12b illustrates the sound absorption mechanism of the composite material. The left side presents an overall schematic of sound wave propagation within the composite material, while the right side provides a detailed mechanism of horizontal sound wave propagation. In the diagram, red lines represent incident sound waves, and blue lines denote reflected sound waves. When sound waves penetrate the composite material, a portion of the sound energy is converted into kinetic and thermal energy, while the remaining portion continues to diffuse and propagate. The presence of air gaps between adjacent layers and the dissimilarity of materials in different layers create impedance mismatches at the interfaces, increasing the probability of sound wave reflection at these boundaries [51]. Therefore, the sound propagation path in the sound-absorbing composite increases, resulting in more air friction, and effectively dissipates the energy of the sound wave. This unique layered structure is likely the main reason for the discrepancies between the experimental and simulated data for the composite materials. Thus, whether the three-parameter model is applicable to composite sound-absorbing materials still requires extensive experimental validation. Furthermore, the model may need to be optimized for different types of porous materials to better account for the specific structural characteristics of composite materials.

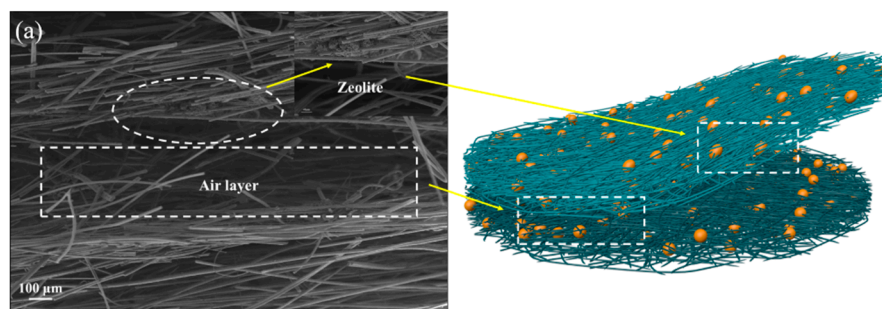


Figure 12. Cont.

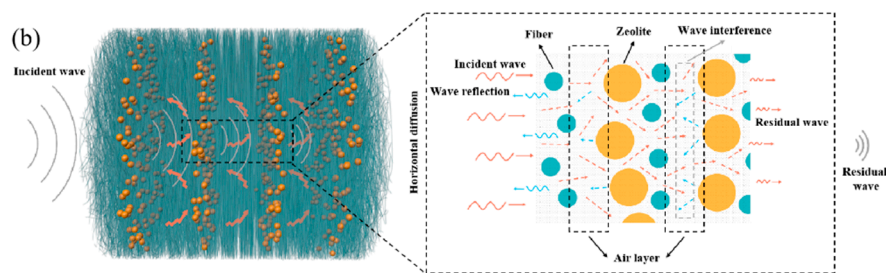


Figure 12. (a) Interlayer microstructure of composite materials; (b) Schematic illustration of the sound absorption mechanism of composite materials.

5. Conclusions

This study, based on the three-parameter approximation of the JCAL model, investigated the effects of fiber diameter variation and zeolite particle addition on the pore size distribution of porous materials and analyzed their influence on the acoustic performance of glass fiber porous materials. The following conclusions were drawn:

Smaller pore sizes improve the low-frequency sound absorption performance of glass fiber porous materials. However, excessively small pores increase density and flow resistivity, resulting in significant sound wave reflection and negatively impacting acoustic performance. Thus, the sound absorption performance of fiber porous materials exhibits an optimal pore size range, with the best acoustic performance observed for pores between 60 and 80 μm .

Both density and fiber diameter influence pore size and, consequently, the acoustic performance of sound-absorbing materials. As the density of fiber porous materials increases, the median pore size decreases, leading to improved mid-to-low-frequency sound absorption performance. The best acoustic performance is achieved at a density of 120 kg/m^3 . At the same density, smaller fiber diameters reduce pore size and enhance acoustic performance.

For composite porous materials made of glass fibers and zeolite particles, zeolite replacement reduces acoustic performance at low density. Conversely, at higher densities, a small amount of zeolite improves acoustic performance by optimizing the pore structure. The best sound absorption performance is achieved at a density of 120 kg/m^3 with a zeolite replacement ratio of 10%, yielding a noise reduction coefficient (NRC) of 0.65.

The comparison between experimental and simulated results using the JCAL three-parameter model shows a high degree of agreement for single-fiber porous materials. However, for composite materials, discrepancies arise due to their complex microstructural changes. Particularly in composite materials, the interfacial structures between layers and the interaction between fibers and particles introduce complexities in predicting acoustic impedance, leading to deviations between experimental and simulated data.

Supplementary Materials: The following supporting information can be downloaded at: <https://www.mdpi.com/article/10.3390/app15063104/s1>, Figure S1: Sound absorption coefficient curves under different median pore size; Figure S2: Schematic Diagram of the Sound Absorption Testing Device; Figure S3: SEM image of potassium silicate attached fiber surface. Table S1: Averaged normalized mass percentages measured by EDS; Table S2: Median pore size of composite porous materials with different volumetric weight, Table S3: NRC of single fiber porous material under different volumetric weight, Table S4: NRC of fiber composite porous materials under different volumetric weight.

Author Contributions: H.S.: writing—original draft, visualization, software, investigation, data curation; J.X.: writing—review and editing; D.L.: conceptualization; Y.F. (Yaohan Feng): formal analysis; P.T.: writing—review and editing, resources, supervision, funding acquisition; Y.F. (Ya Feng):

writing—review and editing, supervision, resources, funding acquisition. All authors have read and agreed to the published version of the manuscript.

Funding: This work was funded and supported by the National Natural Science Foundation of China (Grant No. 52108245) and the National Key R&D Program of China (Grant No. 2023YFC3806301-03).

Institutional Review Board Statement: Not applicable.

Informed Consent Statement: Not applicable.

Data Availability Statement: The original contributions presented in this study are included in the article/Supplementary Materials. Further inquiries can be directed to the corresponding authors.

Conflicts of Interest: Author Junhuai Xu is a formal employee of China Southwest Architecture Design and Research Institute Co., Ltd., and also holds a part-time position at its subsidiary, CSWADI (Sichuan) Science and Technology Co., Ltd. The remaining authors declare that the research was conducted in the absence of any commercial or financial relationships that could be construed as a potential conflict of interest.

References

1. Montenegro, A.L.; Rey-Gozaló, G.; Arenas, J.P.; Suárez, E. Streets classification models by urban features for road traffic noise estimation. *Sci. Total Environ.* **2024**, *932*, 173005. [[CrossRef](#)]
2. Bulkin, V.V.; Khromulina, T.D.; Kirillov, I.N. Analysis of the Acoustically Noise Situation in an Urbanized Area in the Presence of Vehicular and Industrial Noise. *IOP Conf. Ser. Earth Environ. Sci.* **2019**, *272*, 022237. [[CrossRef](#)]
3. Cao, L.; Fu, Q.; Si, Y.; Ding, B.; Yu, J. Porous materials for sound absorption. *Compos. Commun.* **2018**, *10*, 25–35. [[CrossRef](#)]
4. Tang, X.; Yan, X. Acoustic energy absorption properties of fibrous materials: A review. *Compos. Part A Appl. Sci. Manuf.* **2017**, *101*, 360–380. [[CrossRef](#)]
5. Sharma, S.; Sudhakara, P.; Singh, J.; Singh, S.; Singh, G. Emerging progressive developments in the fibrous composites for acoustic applications. *J. Manuf. Process.* **2023**, *102*, 443–477. [[CrossRef](#)]
6. Wang, Z.; Novack, T.; Yan, Y.; Zipf, A. Quiet Route Planning for Pedestrians in Traffic Noise Polluted Environments. *IEEE Trans. Intell. Transp. Syst.* **2021**, *22*, 7573–7584. [[CrossRef](#)]
7. Berkhout, B.W. Anthropogenic noise pollution and wildlife diseases. *Trends Parasitol.* **2023**, *39*, 181–190. [[CrossRef](#)]
8. Sordello, R. Evidence of the environmental impact of noise pollution on biodiversity: A systematic map protocol. *Environ. Evid.* **2019**, *8*, 8. [[CrossRef](#)]
9. King, E.A. Here, There, and Everywhere: How the SDGs Must Include Noise Pollution in Their Development Challenges. *Environ. Sci. Policy Sustain. Dev.* **2022**, *64*, 17–32. [[CrossRef](#)]
10. Adewale, B.A.; Stephanie, M. Investigation of The Impact of Noise Control Strategies in Sustainable Building Design. *IOP Conf. Ser. Earth Environ. Sci.* **2022**, *1054*, 012033. [[CrossRef](#)]
11. Yang, W.; Jeon, J.Y. Design strategies and elements of building envelope for urban acoustic environment. *Build. Environ.* **2020**, *182*, 107121. [[CrossRef](#)]
12. Zhang, X.; Zhou, S. Building a City with Low Noise Pollution: Exploring the Mental Health Effect Thresholds of Spatiotemporal Environmental Noise Exposure and Urban Planning Solution. *Int. J. Environ. Res. Public Health* **2023**, *20*, 4222. [[CrossRef](#)]
13. Radicchi, A. Quietness as a commons: Integrating soundscape in urban planning for the environmentally just city. *J. Acoust. Soc. Am.* **2017**, *142*, 2671. [[CrossRef](#)]
14. Morillas, J.M.B.; Gozaló, G.R.; González, D.M.; Moraga, P.A.; Vélchez-Gómez, R. Noise Pollution and Urban Planning. *Curr. Pollut. Rep.* **2018**, *4*, 208–219. [[CrossRef](#)]
15. Liu, R.; Hou, L.; Zhou, W.; Chen, Y. Design, fabrication and sound absorption performance investigation of porous copper fiber sintered sheets with rough surface. *Appl. Acoust.* **2020**, *170*, 107525. [[CrossRef](#)]
16. Xi, Z.; Zhu, J.; Tang, H.; Ao, Q.; Zhi, H.; Wang, J.; Li, C. Progress of Application Researches of Porous Fiber Metals. *Materials* **2011**, *4*, 816–824. [[CrossRef](#)] [[PubMed](#)]
17. Venegas, R.; Umnova, O. Acoustical properties of double porosity granular materials. *J. Acoust. Soc. Am.* **2011**, *130*, 2765–2776. [[CrossRef](#)]
18. Liu, X.; Yan, X.; Zhang, H. Effects of pore structure on sound absorption of kapok-based fiber nonwoven fabrics at low frequency. *Text. Res. J.* **2016**, *86*, 755–764. [[CrossRef](#)]
19. Dong, C.; Liu, Z.; Liu, X.; Pierce, R.S.; Yi, X. Sound absorption performance of folded structures prepared from woven prepreg and porous material composites. *Appl. Acoust.* **2023**, *212*, 109591. [[CrossRef](#)]

20. Hirose, K. Numerical study on the influence of fiber cross-sectional shapes on the sound absorption efficiency of fibrous porous materials. *Appl. Acoust.* **2020**, *164*, 107222. [[CrossRef](#)]
21. Puguang, J.M.C.; Agbayani, D.B.A.; Sadural, A.J.V.; Kim, H. Enhanced Low Frequency Sound Absorption of Bilayer Nanocomposite Acoustic Absorber Laminated with Microperforated Nanofiber Felt. *ACS Appl. Polym. Mater.* **2023**, *5*, 8880–8889. [[CrossRef](#)]
22. Chen, J.H.; Liu, P.S.; Sun, J.X. Sound absorption performance of a lightweight ceramic foam. *Ceram. Int.* **2020**, *46*, 22699–22708. [[CrossRef](#)]
23. Chen, J. Research Progress on Sound Absorption of Fiber-Based Materials and Their Composites. *Fibers Polym.* **2024**, *25*, 4529–4555. [[CrossRef](#)]
24. Delany, M.E.; Bazley, E.N. Acoustical properties of fibrous absorbent materials. *Appl. Acoust.* **1970**, *3*, 105–116. [[CrossRef](#)]
25. Miki, Y. Acoustical properties of porous materials. Modifications of Delany-Bazley models. *J. Acoust. Soc. Jpn. (E)* **1990**, *11*, 19–24. [[CrossRef](#)]
26. Komatsu, T. Improvement of the Delany-Bazley and Miki models for fibrous sound-absorbing materials. *Acoust. Sci. Tech.* **2008**, *29*, 121–129. [[CrossRef](#)]
27. He, Y.; Hu, C.; Wang, J.; Yao, Z.; Cai, J. Optimized Delany-Bazley sound absorption model of flat polyester fiber. *Tech. Acoust.* **2022**, *41*, 252–256. [[CrossRef](#)]
28. Allard, J.-F.; Champoux, Y. New empirical equations for sound propagation in rigid frame fibrous materials. *J. Acoust. Soc. Am.* **1992**, *91*, 3346–3353. [[CrossRef](#)]
29. Kino, N. Ultrasonic measurements of the two characteristic lengths in fibrous materials. *Appl. Acoust.* **2007**, *68*, 1427–1438. [[CrossRef](#)]
30. Kino, N. Further investigations of empirical improvements to the Johnson–Champoux–Allard model. *Appl. Acoust.* **2015**, *96*, 153–170. [[CrossRef](#)]
31. Champoux, Y.; Allard, J.-F. Dynamic tortuosity and bulk modulus in air-saturated porous media. *J. Appl. Phys.* **1991**, *70*, 1975–1979. [[CrossRef](#)]
32. Pride, S.R.; Morgan, F.D.; Gangi, A.F. Drag forces of porous-medium acoustics. *Phys. Rev. B* **1993**, *47*, 4964–4978. [[CrossRef](#)]
33. Horoshenkov, K.V.; Hurrell, A.; Groby, J.-P. A three-parameter analytical model for the acoustical properties of porous media. *J. Acoust. Soc. Am.* **2019**, *145*, 2512–2517. [[CrossRef](#)] [[PubMed](#)]
34. Nguyen, C.T.; Langlois, V.; Guilleminot, J.; Duval, A.; Perrot, C. Effect of pore size polydispersity on the acoustic properties of high-porosity solid foams. *Phys. Fluids* **2024**, *36*, 047101. [[CrossRef](#)]
35. Nguyen, C.T.; Li, D.; Xiong, Z.; He, M.; Gautron, L.; Duval, A.; Perrot, C. Structure-property relationships of polydisperse open-cell foams: Application to melamine foams. *Acta Acust.* **2024**, *8*, 54. [[CrossRef](#)]
36. Gao, J.; Dong, F.; Jia, J.; Tan, C. Calibration-free temperature monitoring of pulverized coal powder based on the dual-mode acoustic tomography. *Powder Technol.* **2024**, *448*, 120220.
37. Saati, F.; Hoppe, K.-A.; Marburg, S.; Horoshenkov, K.V. The accuracy of some models to predict the acoustical properties of granular media. *Appl. Acoust.* **2022**, *185*, 108358. [[CrossRef](#)]
38. Hurrell, A.; Horoshenkov, K.V.; King, S.G.; Stolojon, V. On the relationship of the observed acoustical and related non-acoustical behaviours of nanofibers membranes using Biot- and Darcy-type models. *Appl. Acoust.* **2021**, *179*, 108075. [[CrossRef](#)]
39. Begum, H.; Horoshenkov, K.V. Acoustical Properties of Fiberglass Blankets Impregnated with Silica Aerogel. *Appl. Sci.* **2021**, *11*, 4593. [[CrossRef](#)]
40. Pan, Q.; Hu, J.; Hu, C.; Yan, Y. Reproduction and characterization of carbon nanotubes coated on expanded perlite as sound absorption composite materials. *Mater. Sci. Eng. B* **2023**, *296*, 116697. [[CrossRef](#)]
41. Wei, Z.; Weavers, L.K. Combining COMSOL modeling with acoustic pressure maps to design sono-reactors. *Ultrason. Sonochemistry* **2016**, *31*, 490–498. [[CrossRef](#)] [[PubMed](#)]
42. ASTM F316-03; Standard Test Methods for Pore Size Characteristics of Membrane Filters by Bubble Point and Mean Flow Pore Test. ASTM: West Conshohocken, PA, USA, 2019.
43. GB/T 18696.2-2002; Acoustics—Determination of Sound Absorption Coefficient and Impedance in Impedance tubes—Part 2: Transfer Function Method. National Standard of the People’s Republic of China: Beijing, China, 2002.
44. ASTM C634-13 (2021); Standard Terminology Relating to Building and Environmental Acoustics. ASTM: West Conshohocken, PA, USA, 2021.
45. Tascan, M.; Vaughn, E.A.; Stevens, K.A.; Brown, P.J. Effects of total surface area and fabric density on the acoustical behavior of traditional thermal-bonded highloft nonwoven fabrics. *J. Text. Inst.* **2011**, *102*, 746–751. [[CrossRef](#)]
46. Bai, H.; Qian, X.; Fan, J.; Qian, Y.; Duo, Y.; Liu, Y.; Wang, X. Computing Pore Size Distribution in Non-woven Fibrous Filter Media. *Fibers Polym.* **2020**, *21*, 196–203. [[CrossRef](#)]
47. Everett, D.H. Manual of Symbols and Terminology for Physicochemical Quantities and Units, Appendix II: Definitions, Terminology and Symbols in Colloid and Surface Chemistry. *Pure Appl. Chem.* **1972**, *31*, 577–638. [[CrossRef](#)]

48. Xin, F.; Ma, X.; Liu, X.; Zhang, C. A multiscale theoretical approach for the sound absorption of slit-perforated double porosity materials. *Compos. Struct.* **2019**, *223*, 110919. [[CrossRef](#)]
49. Wang, Y.; Chen, Y.; Yang, S.; Liu, J.; Xie, H. Experimental Study on Gypsum-based Sound-absorbing Ceramsite Materials. *Chongqing Archit.* **2020**, *19*, 25–28.
50. Ishikawa, S.; Hirata, R.; Kijimoto, S. Improved effectiveness of acoustic absorbing materials by using air layers in a one-dimensional tube. *Appl. Acoust.* **2021**, *178*, 107984. [[CrossRef](#)]
51. Jiang, X.; Wang, Z.; Yang, Z.; Zhang, F.; You, F.; Yao, C. Structural Design and Sound Absorption Properties of Nitrile Butadiene Rubber-Polyurethane Foam Composites with Stratified Structure. *Polymers* **2018**, *10*, 946. [[CrossRef](#)]

Disclaimer/Publisher's Note: The statements, opinions and data contained in all publications are solely those of the individual author(s) and contributor(s) and not of MDPI and/or the editor(s). MDPI and/or the editor(s) disclaim responsibility for any injury to people or property resulting from any ideas, methods, instructions or products referred to in the content.